

Stirring, folding and mixing in electromagnetically driven flows of controlled geometry and acceleration (experiments and numerical simulations)

L. Rossi, J.M. Garcia de la Cruz, S. Bocquet and S. Lardeau

Department of Aeronautics

Imperial College London

Prince consort road, SW7 2AZ, London United Kingdom

l.rossi@imperial.ac.uk

ABSTRACT

Prior to study mixing via the temporal evolution of passive scalars, the authors attempt to isolate the key mechanisms to stir flows of controlled geometries. The stretching properties of these flows are studied using a strain rate approach. The folding and lamination rate properties are then quantified and explored using a new approach proposed by (Rossi 2009) which is based on the spatial variation of the Lagrangian angular velocity. The main emphasis of this paper is set on the determination of folding and lamination rate of multi- and one-scale flows using this novel approach. Such results are complemented by the description of these flows, including: visualisations, velocity, acceleration and strain rate fields. This quantification of folding and lamination rates is found to highlight subtle and important flow properties for both multi- and one-scale flows. It permits to identify scales and rates of lamination. Also, the good agreement between visualisation based on the deformation of a mesh and Lagrangian averaging of folding and lamination rate intensity is striking. This is extremely encouraging to pursue the exploration of this laminating approach and its offspring for mixing studies in complex flows.

INTRODUCTION

Mixing is a crucial process in a broad range of flows, ranging from geophysical flows to micro-flows. Large-scale examples are combustors and chemical reactors in which controlled mixing is required to improve efficiency. For those large and intermediate-scale apparatus, the Reynolds number is high enough for the flow to develop natural turbulence which is usually considered as a good mixer. As the scale reduces, so does the Reynolds number. For micro-applications, where the Reynolds number is of the order of unity, the flow is laminar. The main challenge hence remains in enhancing mixing by mimicking the stirring mechanisms (e.g. stretching and folding) of large-scale mixers, i.e. trying to recover a pseudo turbulent stirring using an ordered stirrer, while minimizing the energy input. Recent works by the authors have addressed some of those challenges by generating a new class of multi-scale laminar flow controlled by multi-scale electromagnetic forcing. The particular arrangement of the magnets leads to interesting turbulent-like properties. We briefly mention few of them hereafter. i) The flow exhibits a power-law energy spectrum $E(k) \sim k^{-p}$, with the exponent $p = 2.5$ prescribed by this arrangement (Hascoet et al 2008; Rossi et al 2006a). This value of p is different from 2D

turbulent flows forced at small scales ($p = 5/3$) or large-scale ($p = 3$) (Tabeling 2002). ii) A Richardson-like diffusion (Richardson 1926), driven by the multi-scale distribution of high stretching regions, with the mean square separation of pairs of fluid element evolving like $\Delta^2 \sim t^3$ once all scales are distinct and ordered, (Rossi et al 2006b). Recently, the authors have used numerical simulations based on 3D DNS to analyze the driving mechanism of these flows, (Lardeau et al 2008). Noticeably, they have shown the interlaced action of forcing and pressure terms to generate and transfer momentum and also the importance of the discretisation of the shallow layer of brine along the wall normal direction to properly simulate the shear and the electromagnetic forces. Other 3D numerical approaches can be found in (Akkermans et al 2008; Kenjeres 2008; Kenjeres et al 2009).

It is well known that combinations of stretching and folding can produce exponential growth of interfaces as illustrated by the baker process discussed by Reynolds in 1893 (Reynolds 1893). Such approach is mainly explored in low Reynolds number flows whilst this mechanism should also occur in turbulent flows, for example during topological changes. This may be due to the absence of accepted definitions to characterise the lamination within flows. A new mechanism to explore folding and lamination rate has recently been proposed (Rossi 2009). Such definition permits to identify and quantify lamination rates and can then be applied to canonical flows with controlled geometry and acceleration. Consequently, the authors design low Reynolds number complex flows to control changes in the flows geometry/topology and investigate the stirring properties of basic building blocks (Rossi et al 2009). The dynamic control of these building blocks is intended to design, in space and time, complex flows with different properties, such as for instance, the transition from cat's eyes (figure of height) to "single eddy". To this aim, the geometry of the flow is designed and controlled by varying the geometry of the forcing.

The first part of this paper briefly introduces the principles of the generation of these flows driven by electromagnetic forcing, their realisation, measure and simulation. In the second part of this paper, the geometry of these flows is briefly illustrated via visualisations complemented by both velocity and Lagrangian acceleration fields. Then the stirring properties of these flows are explored and the quantification of lamination rates proposed by (Rossi 2009) is applied to multi- and one-scale flows.

FLOWS DRIVEN BY ELECTROMAGNETIC FORCING

Electromagnetically driven flows

Shallow layer brine flows are driven by electromagnetic forces, $\mathbf{f}(\mathbf{x})$, with $\mathbf{f}(\mathbf{x}) = \mathbf{j} \times \mathbf{B}$, where $\mathbf{j}(\mathbf{x})$ is the electrical current density and $\mathbf{B}(\mathbf{x})$ is the magnetic field, given by the induction equation $\frac{\partial \mathbf{B}}{\partial t} = \nabla \times (\mathbf{u} \times \mathbf{B}) + \frac{1}{\mu\sigma} \nabla^2 \mathbf{B}$ and Ohm's law $\mathbf{j} = \sigma(\mathbf{u} \times \mathbf{B} + \mathbf{E})$; where \mathbf{u} is the velocity vector, μ is the magnetic permeability, σ the electrical conductivity and \mathbf{E} the imposed external electric field. If σ is low (as is the case here) and the velocity moderate, the magnetic Reynolds number, defined as $Re_m = \sigma \mu u l$ is very small compared to 1. In the case of steady magnetic field the induction equation can be then approximated by: $\nabla^2 \mathbf{B} = 0$. In addition, the induced electrical current ($\sigma \mathbf{u} \times \mathbf{B}$) is neglected as $uB \ll E$. The electric density is then imposed by the external electric field, $\mathbf{j} \cong \sigma \mathbf{E}$. The electromagnetic forces are consequently assumed to be independent of the flow velocity. The Hartmann number is larger than one, for all flows considered hereafter, meaning that the electromagnetic forces are high enough to overcome the damping forces due to viscosity (essentially due to the bottom friction). In the present case, the forcing is not a perturbation of an existing flow: without the electromagnetic forcing, there is no flow. The flow is initially at rest. When the current is switched on, the flow velocity increases until it reaches a quasi-steady state. Flow configurations, experiments and numerical simulations are here discussed only when this quasi-steady state is reached.

The general setting is shown on Fig. 1. The magnetic induction of the permanent magnets is $Br = 0.68T$, the salt concentration is $158g/l$, the viscosity ν is $1.36 \cdot 10^{-6}m^2s^{-1}$, the density ρ is $1105kgm^{-3}$ and its conductivity, $\sigma = 16.6Sm^{-1}$ and the magnetic permeability $\mu \approx \mu_0 = 4\pi \cdot 10^{-7}VsA^{-1}m^{-1}$.



Fig. 1: Schematic of the experimental rig

Two different forcing configurations are considered: a single pair of magnets, Fig. (2a), for different angle α , and a multi-scale arrangement of magnets, Fig. (2b). For the single pair of magnets, the two square permanent magnets are 40mm aside. And the brine thickness is $H=6mm$. The electrical current density, $\mathbf{j} = I/S$ where I is the electrical current and S the cross section of the brine is kept constant at a value of about $\mathbf{j} = 13.5A/m^2$ ($I = 48.6mA$). This leads to electromagnetic forces of constant intensity with $f_{rms} = 3.26Nm^{-3}$. For the multi-scale forcing the magnets sizes are 10mm, 40mm and 160mm (Rossi et al 2006a) and the brine thickness is $H=5mm$. The flows are driven by electromagnetic forces of quasi-constant mean intensity within the brine above each magnet. The root mean square of the forces computed over the numerical domain is varied from $\frac{1}{\rho} f_{rms} = 5.72 mm/s^2$ when $I = 0.06A$ to $\frac{1}{\rho} f_{rms} = 66.68 mm/s^2$ when $I = 0.7A$.

The notation + denotes dimensionless number built using the characteristics of the electromagnetic forcing. The size of the medium magnets, L_{M40} , which is common to both configurations, is chosen as reference length scale,

$\mathcal{L}^+ = \mathcal{L}/L_{M40}$. The folding and lamination rate is made dimensionless using as reference the ratio of acceleration and velocity $F_{olref} = a_{ref}/u_{ref} = \sqrt{\frac{2f_{rms}}{\rho L_M}}$ with $F_{ol}^+ = F_{ol}/F_{olref}$ where L_M is the size of the largest magnets of the forcing configuration. Also, the strain rate reference is $s_{ref} = \sqrt{\frac{f_{rms}}{2\rho L_M}}$ and $s^+ = s/s_{ref}$ is the dimensionless strain rate. The velocity and acceleration are normalised by the root mean square velocity and acceleration computed over the experimental or numerical domains. They are respectively noted $\mathbf{u}^* = \mathbf{u}/u_{rms}$ and $\mathbf{a}^* = \mathbf{a}/a_{rms}$.

Table 1: characteristic scales

	One-scale			Multi-scale	
	0°	15°	90°	$Re_e = 3$	$Re_e = 25$
u_{rms} (mm/s)	1.73	1.8	1.63	0.867	6.52
a_{rms} (mm/s ²)	0.291	0.297	0.265	0.034	1.22
F_{olref} (rad/s)	0.192	0.192	0.192	0.0423	0.126
s_{ref} (1/s)	0.384	0.384	0.384	0.0845	0.289

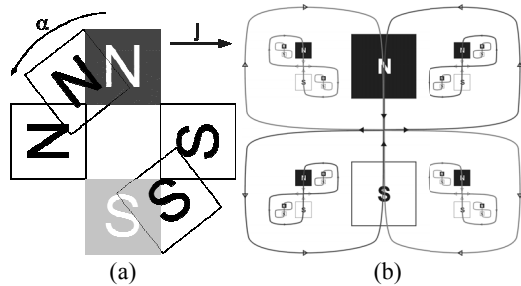


Fig. 2: Distributions of permanent magnets underneath the wall, one- (a) and multi- (b) scale configurations

Experiments

Experiments are performed in a tank (800mmx600mm), smaller than the one used in (Rossi et al 2006a). The brine-supporting wall is checked so as to keep it straight and horizontal, with a standard deviation of about 0.12mm. Real-time PIV measurements are performed using a 14Hz camera (2048 × 2048pixel², 14bit) and a picture frame of 441 × 441mm². Pliolite DF01 (100µm < diameter < 200µm) is used to seed the flow and Particle Image Velocimetry (PIV) post-processing is performed with an in-house code (iterative method with sub-pixel accuracy). The maximal displacement is about 17 pixels per frame and the smallest correlation window is of 16 pixels by 16 pixels. Typically, the values of the correlation coefficients of these PIV measurements are about 0.9. PIV fields are computed with a grid of 222×222 points. The corresponding distance between two velocity points is of 8 pixels. This gives more than 20 × 20 points above each magnets and a final correlation window size about 12 times smaller than the magnet length. Taking advantage of this PIV data resolved in space and time, we extract the corresponding acceleration fields using the PTVA algorithm (Ferrari & Rossi 2008) and virtual particle tracking. For more details, see (Rossi et al 2009).

Numerical Simulations

Computations are carried out with a finite difference code, using 6th-order compact scheme for spatial discretization and 3rd order Runge-Kutta scheme for time derivatives. Poisson equation is solved directly using

Fourier decomposition. The electromagnetic forcing model is based on an analytical model (Akoun & Yonnet 1984; Thibault & Rossi 2003), considering the 3D distribution of the permanent magnets. The numerical simulations are carried out and validated for different intensity of the forcing, geometries and brine thickness which are chosen accordingly to experiments. This provides a complementary set of statistics and the full 3D description of our flows. For more details see (Lardeau et al 2008; Rossi et al 2009).

STIRRING IN FLOWS WITH CONTROLLED GEOMETRIES AND ACCELERATION

Stretching and folding

Prior to study the mixing properties of these flows the authors attempt to identify and quantify their stirring properties, e.g. stretching, folding, swapping and cutting. In particular, this paper focuses on the exploration of folding and lamination rate and is based on the new approach proposed by (Rossi 2009) to define and quantify this rate.

The Fundamental mechanism to explore lamination and folding rates relies on the quantification of the action of the forces applied on a material line to turn it at different angular speeds. The Lagrangian acceleration, \mathbf{a} , represents the forces exerted on a particle-fluid by its environment and governs the alteration in direction and intensity of its Lagrangian velocity. Consequently, this new approach considers the alignment between the velocity and the Lagrangian acceleration, and in particular the component of the acceleration, \mathbf{a}_p , perpendicular to the velocity (rather than the vorticity) to determine the local Lagrangian angular velocity, i.e. the speed of change of direction of the Lagrangian velocity vector. This rate corresponds to an angular velocity, $\dot{\theta}$, around the rotation vector, \mathbf{e}_f , which are defined by equations: $\dot{\theta} = \sqrt{\mathbf{a}_p \cdot \mathbf{a}_p / \mathbf{u} \cdot \mathbf{u}}$ and $\mathbf{e}_f = \mathbf{u} \times \mathbf{a}_p / \|\mathbf{u} \times \mathbf{a}_p\|$. The folding and lamination rate of a material line element, $d\ell$, around the direction \mathbf{e}_f is now defined using the spatial variation of $\dot{\theta}$ along $d\ell$. Such choice is also supported by (Bajer et al 2001) who have recently shown that differential rotation is key to accelerate diffusion in the centre of analytical vortices. To perform a global quantification, the folding rate intensity is here simplified to $\dot{F}_{ol} = \|\nabla \dot{\theta}\| \ell$ where ℓ is a typical length-scale. Also the domain over which the lamination is coherent is of interest to define the laminating properties of a flow/mixer. To this aim, $\dot{\theta} \mathbf{e}_f \cdot \mathbf{y}$ is coarse grained by averaging within mobile windows of size \mathcal{L} [\mathbf{y} is the direction perpendicular to the measurement plan and $\dot{\theta} \mathbf{e}_f \cdot \mathbf{y} = \pm 1$ in 2D]. The corresponding laminating rate intensity is then computed over these coarse grained fields with $\ell = \mathcal{L}$. This approach permits to extract the laminating rate of the flows at typical length scales. For more details, see (Rossi 2009).

The stretching is illustrated via the quantification of strain rate maps. Complemented by the folding and lamination rate maps it permits to discuss and compare these two stirring properties.

Multi-scale flow

Figures 3, 4 and 5 give DNS results with multi-scale forcing. (Lardeau et al 2008). The visualisation presented in

Fig. 3 shows the typical structure driven by these multi-scale forcing. The multi-scale generation of counter jets creates a structure of flows within flows. Fig. 4 (a and b) gives the velocity and Lagrangian acceleration fields of these flows for two different Reynolds numbers: 3 and 25 with $Re = u_{rms}H/\nu$. Whilst the topology and energy spectra of these multi-scale flows are conserved (Rossi et al 2006a) the distributions of velocity and Lagrangian acceleration intensities clearly evolve with Re . This dependence on Re is also found on both strain and lamination rates. The variation of the strain rate distribution can be related to the variation of pairs dispersion statistics (Lardeau et al 2008; Rossi et al 2006b). Fig. 4d shows the increase of the importance of the large-scale flow (and forcing) in the distribution of the lamination rates. This is confirmed by the distribution of folding rate according to targeted scales given in Fig. 5. For low Re , the lamination rates are more important at the medium scale and a plateau is observed for $Re = 15$. This shows that the lamination rate is sensitive to subtle and important changes in these multi-scale flows. This is encouraging for its use in fundamental and mixing studies.

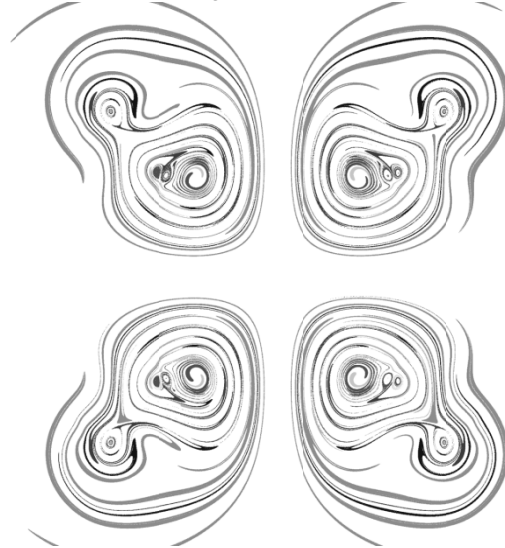


Fig. 3: Visualisation of the multi-scale flow (zoom)

One-scale flow

To illustrate the characterisation of lamination rate, the flows are now simplified to basic building blocks (Rossi et al 2009). The change of geometry/topology is performed by varying the geometry of the forcing: the pair of square permanent magnets are rotated by an angle α , where α corresponds to the orientation of the magnets with respect to the direction normal to the electrical current, Fig. 2. The flow is pumped above the magnets in opposite directions perpendicular to the electrical current. The case $\alpha = 0^\circ$ corresponds to a “straight hyperbolic stagnation point” similar to those forced in the multi-scale distribution. At $\alpha = 15^\circ$, the forcing produces a cat’s eyes and at $\alpha = 90^\circ$ a single eddy. Those geometries are clearly illustrated by figures 7 and 8 (first rows). We should indicate that depending on the electromagnetic forces intensity and the brine thickness some configurations present unsteady flows. Such flows are also under investigations using real time data. Fig. 7(c&d) gives the distribution of velocity and

Lagrangian acceleration fields, with typical geometry and topology for both fields. Critical points are indicated via their eigen directions for hyperbolic and circles for elliptical ones. Fig. 7e gives the strain rate intensities for the three geometries considered. This highlight different stretching properties and distribution according to flows geometry whilst the forcing intensity is kept constant. Fig. 7f gives the folding and lamination rates fields (at $\mathcal{L} = 55mm$). Similarly to velocity and acceleration fields, the lamination rate distribution varies with the flow geometry. It can be noticed that the present Eddying motion of case 90° laminates the flow at a lower rate than cases 0° and 15° . Fig. 6 complement this analyse by giving the distribution of F_{olrms}^+ versus the length-scales, \mathcal{L}^+ . These results show that a maximum of lamination rate combined to a typical length-scale can be identified for each configuration. For hyperbolic cases, this maximum of lamination rate is found for $1.2 \lesssim \mathcal{L}^+ \lesssim 1.4$.

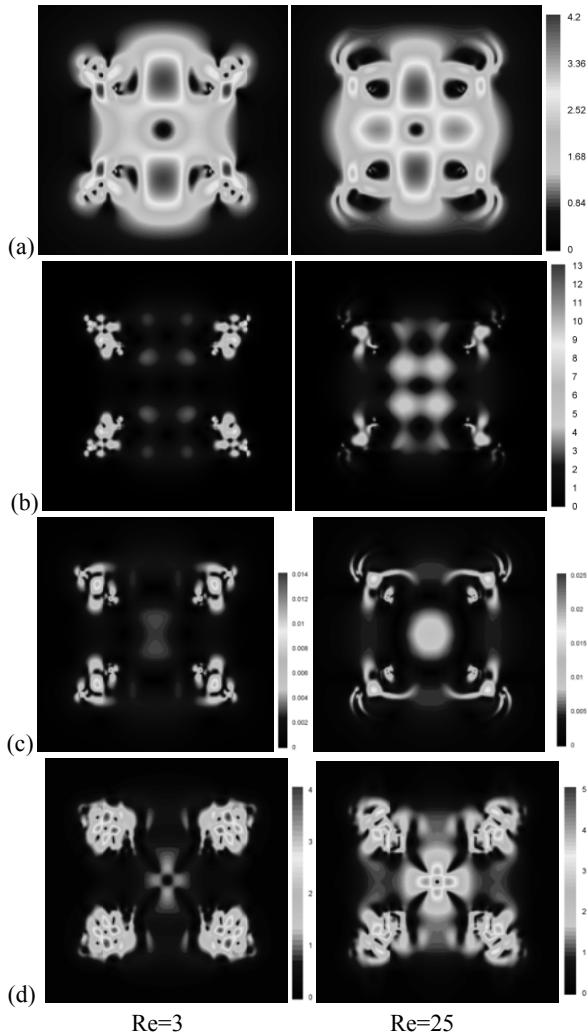


Fig. 4: Spatial distribution of flow intensities for Reynolds numbers 3 and 25: (a) velocity $\|\mathbf{u}^*\|$, (b) Lagrangian acceleration, $\|\mathbf{a}^*\|$ (c) strainrate, s^+ (d) lamination rate, F_{ol}^+ (at $\mathcal{L} = 48mm$). Zoom on a 800mmx800mm domain.

Effective folding and Lamination

The laminating process being an integral process along Lagrangian trajectories, the folding rate intensity is

averaged (over time) along Lagrangian trajectories computed via backward tracking during the time $t^+ = 4.86$. The corresponding distribution of this averaged lamination rate is then compared with the temporal evolution of material lines initially distributed as a regular grid in Fig 8. The good agreement between the visualisation and the distribution of the mean lamination is impressive for the three configurations. This shows that this definition can be used to predict and identify laminated region within flows with important consequences for the fundamental description of flows, mixing and mixers (Rossi 2009).

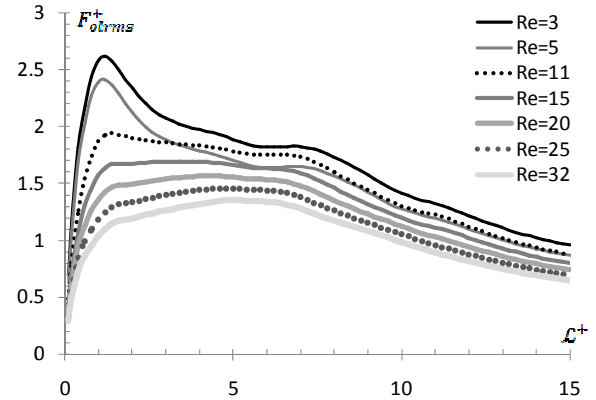


Fig. 5: Folding rate intensity F_{olrms}^+ versus length-scale \mathcal{L}^+ .

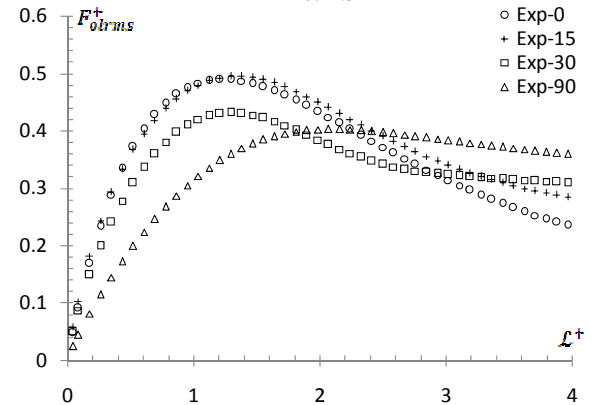


Fig. 6: Lamination rate intensity, F_{olrms}^+ , versus \mathcal{L}^+ .

CONCLUSION

Complementary experiments (e.g. PIV, PTVA) and numerical simulations (3D DNS) are performed and analyzed. The exploration of the proposed folding and lamination rate is supported by both numerical and experimental results. The results presented in this paper are extremely encouraging. They show that different stretching and folding/lamination rates can be quantified for different flow configurations driven by multi- and one- scale forcing. They also highlight that the strain and lamination rates are sensitive to subtle variations within multi-scale flows keeping the same topology and energy spectra. In addition, one-scale experiments show that the detailed control of the flow geometry and topology permits to design building blocks with identified properties in term of strain and laminating rates. This includes the most effective length-scale for the laminating mechanism which appears to be closely related to the flow structure and forcing length-scales.

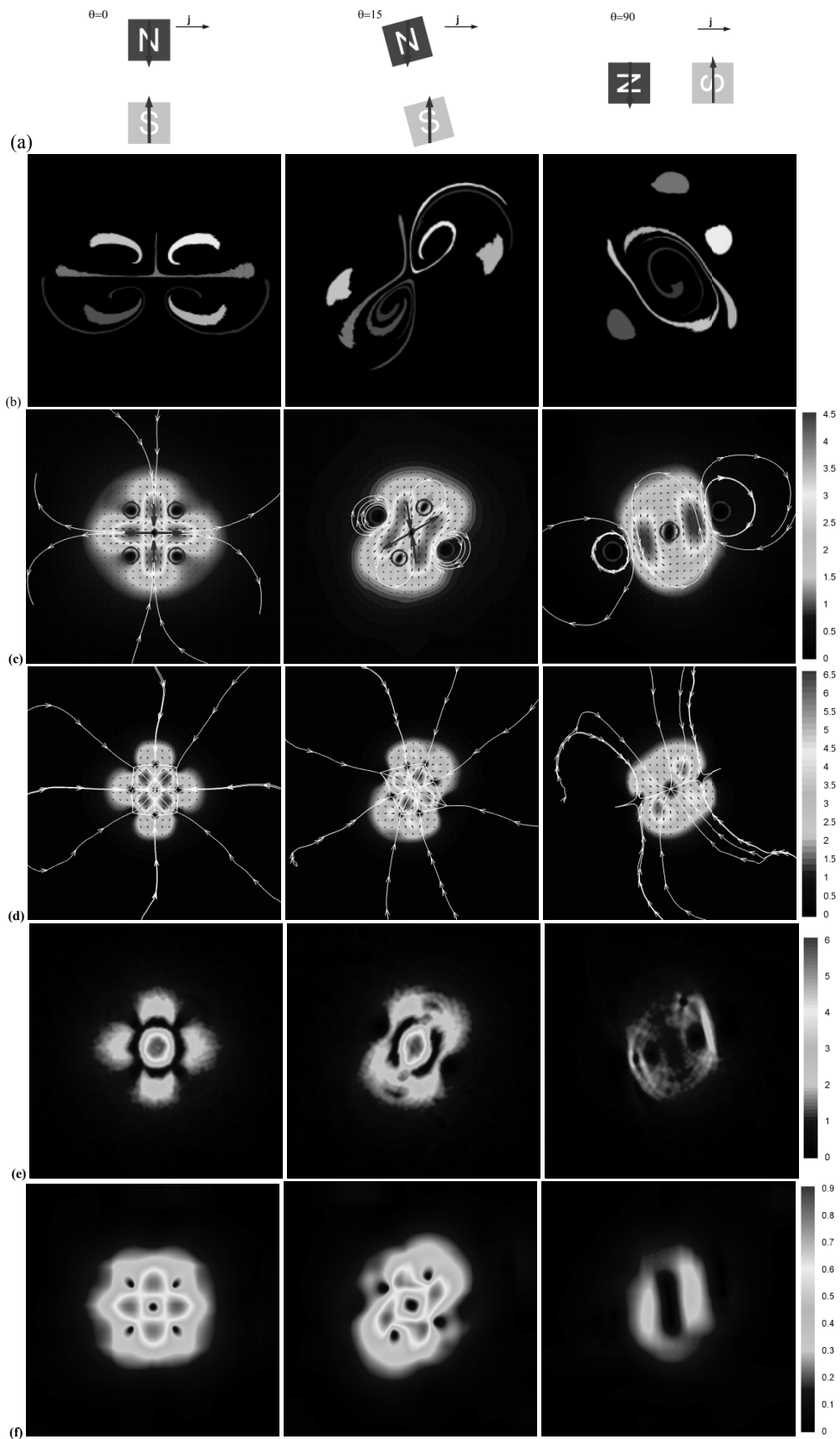


Fig. 7: (a) geometry of the forcing, (b) flow visualisations (c) velocity $\|\mathbf{u}^*\|$, (d) Lagrangian acceleration, $\|\mathbf{a}^*\|$ (e) strainrate, s^+ , (f) lamination rate, F_{ol}^+ .

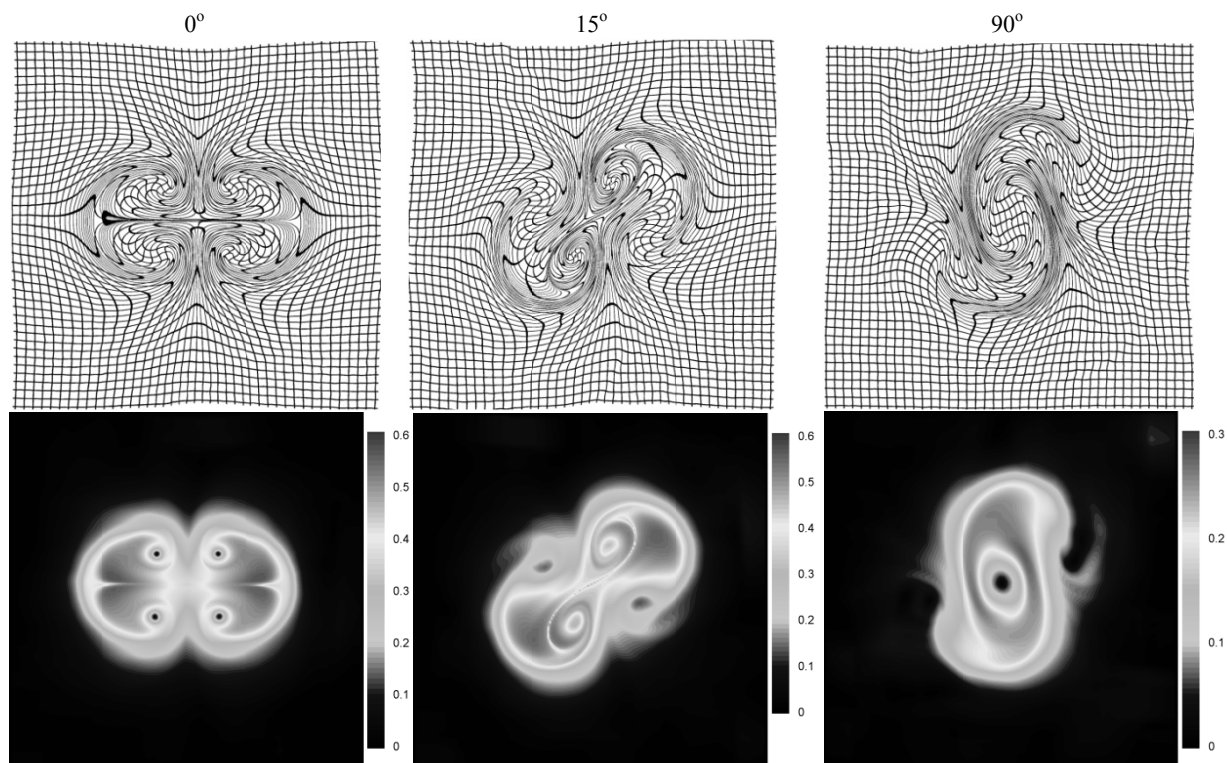


Fig. 8: Visualisation of tracers initially distributed along a regular grid and tracked during the time $t^+ = 4.86$ (first row) and average of the folding rate intensity (at scale: $L^+ = 1.38$) along particle fluid trajectories tracked backward in time during t^+

Currently, the stirring properties (e.g. stretching and folding) of these reference flows are studied and complemented by mixing analyses (e.g. using Light Induced Fluorescence) based on the temporal evolution of a passive scalar's concentration (e.g. time evolution of scalar variance, probability distribution functions) and the temporal evolution of "mixing interfaces". Also, targeted unsteadiness and geometry changes are introduced by dynamically controlling the position of the magnets in time. The dynamic control of the flow geometry/topology is intended to allow the authors to control the stretching and folding/lamination with important consequences for mixing processes and the generation of pseudo turbulent stirrers. Updated results should be included in the conference talk.

The authors acknowledge the support of the EPSRC and the Royal Society to this work.

References

Akkermans RAD, Cieslik AR, Kamp LPJ, Trieling RR, Clercx HJH, Heijst GJFv. 2008. The three-dimensional structure of an electromagnetically generated dipolar vortex in a shallow fluid layer. *Physics of Fluids* 20:116601

Akoun G, Yonnet JP. 1984. 3D analytical calculation of the forces exerted between two cuboidal magnets. *IEEE Transaction on magnetics* 20:1962-4

Bajer K, Bassom AP, Gilbert AD. 2001. Accelerated diffusion in the centre of a vortex. *J. Fluid Mech.* 437:395-411

Ferrari S, Rossi L. 2008. Particle tracking velocimetry and accelerometry (PTVA) measurements applied to quasi-two-dimensional multi-scale flows. *Exp. Fluids* 44:873-86

Hascoet E, Rossi L, Vassilicos JC. 2008. Multi-scale flow control for efficient mixing: simulation of electromagnetically forced turbulent-like laminar flows. *IUTAM Symposium on Flow Control and MEMS*:273-7

Kenjeres S. 2008. Electromagnetic enhancement of turbulent heat transfer. *Phys. Rev. E* 78:066309

Kenjeres S, Verdoold J, Tummers MJ, Hanjalic K, Kleijn CR. 2009. Numerical and experimental study of electromagnetically driven vortical flows. *Int. J. Heat Fluid Flow* In Press

Lardeau S, Ferrari S, Rossi L. 2008. Three-dimensional direct numerical simulation of electromagnetically driven multiscale shallow layer flows: Numerical modeling and physical properties. *Phys. Fluids* 20:127101

Reynolds O. 1893. Study of Fluid Motion by means of Coloured Bands. *Proceedings of the Royal Institution of Great Britain* XIV:129-38

Richardson LF. 1926. Atmospheric Diffusion Shown on a Distance-Negighbour Graph. *Proc. R. Soc. Lond. A* 110:709-37

Rossi L. 2009. A mechanism to explore folding and lamination rates. *Submitted to Phys. Rev. Lett.*

Rossi L, Bocquet S, Ferrari S, Garcia de la Cruz JM, Lardeau S. 2009. Control of flow geometry using electromagnetic body forcing. *Int. J. Heat Fluid Flow* In press

Rossi L, Vassilicos JC, Hardalupas Y. 2006a. Electromagnetically controlled multi-scale flows. *J. Fluid Mech.* 558:207 - 42

Rossi L, Vassilicos JC, Hardalupas Y. 2006b. Multiscale Laminar Flows with Turbulentlike Properties. *Phys. Rev. Lett.* 97:144501

Tabeling P. 2002. Two-dimensional turbulence: a physicist approach. *Physics Reports* 362:1-62

Thibault J-P, Rossi L. 2003. Electromagnetic flow control: characteristic numbers and flow regimes of a wall-normal actuator. *J. Phys. D: Applied Physics*:2559-68